




**Chemical disorder induced electronic orders in correlated metals: Rekindled failed-order scenario**Jinning Hou (侯晋宁) <sup>1</sup>, Yuting Tan (谭宇婷) <sup>2</sup>, and Wei Ku (顧威) <sup>1,3,4,\*</sup><sup>1</sup>*Tsung-Dao Lee Institute & School of Physics and Astronomy, Shanghai Jiao Tong University, Shanghai 200240, China*<sup>2</sup>*Condensed Matter Theory Center and Joint Quantum Institute, Department of Physics, University of Maryland, College Park, Maryland 20742, USA*<sup>3</sup>*Key Laboratory of Artificial Structures and Quantum Control (Ministry of Education), Shanghai 200240, China*<sup>4</sup>*Shanghai Branch, Hefei National Laboratory, Shanghai 201315, China*

(Received 2 March 2023; revised 14 March 2024; accepted 19 April 2024; published 8 May 2024)

In strongly correlated metals, long-range magnetic order is sometimes found only upon introduction of a minute amount of disordered nonmagnetic impurities to the unordered clean samples. To explain such anti-intuitive behavior, we propose a “rekindled failed-order” scenario of inducing electronic (magnetic, orbital, or charge) order via chemical or lattice disorder in systems with coexisting local moments and itinerant carriers. By disrupting the damaging long-range quantum fluctuation originating from the itinerant carriers, the electronic order preferred by the local moment can be reestablished. We demonstrate this mechanism using a realistic spin-fermion model and show that the magnetic order can indeed be recovered as a result of enhanced disorder once the length scale of phase coherence of the itinerant carriers becomes shorter than a critical value. The proposed simple idea has a general applicability to strongly correlated metals, and it showcases the rich physics resulting from interplay between mechanisms of multiple length scales.

DOI: [10.1103/PhysRevB.109.195126](https://doi.org/10.1103/PhysRevB.109.195126)**I. INTRODUCTION**

Typically, random disorder is expected to suppress long-range orders in materials, especially those with a characteristic length scale such as antiferromagnetic order, antiferro-orbital order, or charge density order. This is in part because of the damage to quantum phase coherence resulting from the inhomogeneity in density, in addition to the direct disruption of the preferred spatial periodicity of the long-range order. Indeed, in dirtier samples with more impurities, one usually observes weaker magnetic [1–4], superconducting [5–7], and charge [8–11] orders. Correspondingly, one often intuitively seeks cleaner and more uniform samples for stronger long-range orders.

However, some exceptional cases exist in which long-range order, for example magnetic order, can emerge from the introduction of disorders, such as nonmagnetic impurities. A well-known example is the emergence of antiferromagnetic (AFM) order in  $\text{Sr}_2\text{RuO}_4$  [12–15] when a minute amount ( $\sim 3\%$ ) of  $\text{Ru}^{4+}$  is substituted by nonmagnetic  $\text{Ti}^{4+}$  ions. Similarly, iron-based superconductor  $\text{LaFePO}$  also develops antiferromagnetism upon As substitution of P [16–18]. Indications that AFM order could emerge from unordered systems also have been found in both hole- and electron-doped cuprates via nonmagnetic Zn substitution of Cu [19–24]. Similar phenomena are also found in Zn-doped heavy-fermion material  $\text{CeCoIn}_5$  [25]. Such an anti-intuitive behavior appears to contradict the above fundamental consideration of quantum phase coherence, and thus poses a great challenge to our generic basic understanding.

Theoretically, in a strongly correlated and highly polarizable environment, it is natural to expect the development of local effective moments around even nonmagnetic impurities [26–28]. Such an effective moment surely would have a large impact on the local correlation, such as modifying its temporal fluctuation or inducing a spatial standing-wave pattern through reflection against impurities [29–32]. Nonetheless, since these effects are primarily local in nature and centered around random location of the impurities, it is unlikely that they can provide positive contributions to the formation of long-range order, especially those with a characteristic spatial period, such as an antiferromagnetic order. The lack of geometric frustration in these systems also renders the “order-by-disorder” scenario [33–40] inapplicable. Therefore, a generally applicable mechanism for the observed seemingly anti-intuitive behavior is desperately needed for such a long-standing puzzle.

Here, we propose a generic “rekindled failed-order” scenario of inducing electronic order via a small amount of chemical or lattice disorder in strongly correlated metals. Accepting that most of unordered correlated metals only fail to order due to the influence of itinerant carriers [41,42], we suggest that scattering against the impurities can suppress the damaging carrier-induced long-range quantum fluctuation and in turn allow the local moments to order. We demonstrate this generic mechanism using a realistic spin-fermion model derived from  $\text{FeSe}$  as a prototypical case with a failed antiferromagnetic (AFM) order [41]. Using the linear response as a measure of the stability of the AFM ordered state, we find that with a stronger disorder the long-range magnetic order indeed establishes. Further analysis indicates that the main physical effect of impurity scattering is equivalent to shortening the length scale of carrier-induced quantum fluctuation, such that

\*Corresponding author: [weiku@sjtu.edu.cn](mailto:weiku@sjtu.edu.cn)

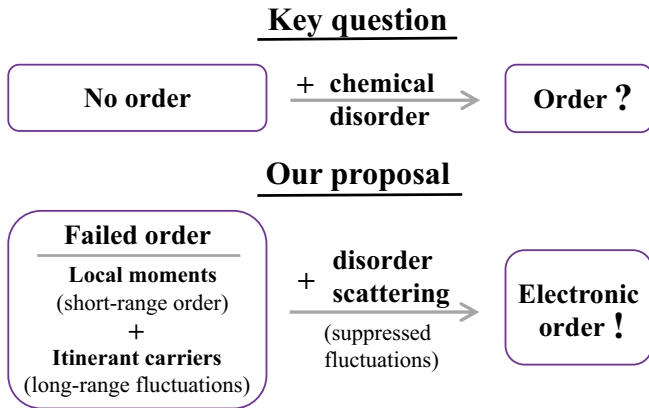


FIG. 1. Key question of the study: How can chemical disorder induce electronic orders in materials? Our “rekindled failed-order” proposal: Disorder induced scattering can suppress the damaging long-range fluctuation of a failed order state and in turn allows the intrinsic electronic order to emerge.

the correlation of local moments is no longer overwhelmed at long range [41]. Our study demonstrates a typical example of the rich interplay between mechanisms of multiple length scales present in most strongly correlated metals, to which our proposed simple idea can be applied in general.

## II. REKINDLED FAILED-ORDER MECHANISM

Figure 1 illustrates our proposed scenario to resolve the long-standing puzzle of electronic ordering upon the introduction of chemical disorder in correlated metals. The key theoretical question here is how disorder, a generic source of incoherence, can induce a coherent long-range order. We make use of the following two generic physical effects that are well established both theoretically and experimentally over the past decades: (1) gapless (metallic) itinerant fermionic carriers induce slowly (power-law) decaying long-range fluctuation in spin [43,44] (and charge [44]) channels, and (2) translational symmetry-breaking disorders damage long-range coherence of itinerant carriers and the fluctuations they introduce [45–48]. Particularly, the first effect has been shown [41] to naturally explain the experimentally well-known consequence that (3) materials with  $d$ - or  $f$ -local moments favoring strong antiferromagnetic correlation typically fail to order magnetically given strong enough metallicity [49,50].

Our proposal is based on such a “failed-order” scenario [41], shown in Fig. 1, in which the long-range order preferred by the correlation between local moments is disrupted by the long-range quantum fluctuation induced by itinerant carriers [42]. Such quantum fluctuation can be quite effective in general since in contrast to the exponential decay of the order-related correlation in three dimensions, the carrier-induced fluctuation has generic power-law decay, due to the discontinuity at the Fermi surface of the fermionic carriers [46–48]. Therefore, by restricting the fluctuation to a short enough finite length scale, we propose that the presence of weak disorder can generally play a positive role in promoting the long-range order of the local moments.

## III. DEMONSTRATION

### A. Spin-fermion model as a demonstration

Below we demonstrate this generic rekindled failed-order mechanism using a representative realistic spin-fermion model, whose family often emerges as the low-energy effective model for a wide range of higher-energy models, such as the large- $U$  regime of the one-band [51] and multiband Hubbard models [52], and the charge transfer regime of the periodic Anderson model [53]. (The previous study on Zn-doped cuprates via  $t - J$  model [54] can also be considered as a specific example of our general proposal.) In fact, upon integrating out the higher-energy intra-atomic charge fluctuation, most strongly correlated materials with strong intra-atomic Coulomb interaction reduce to various forms of spin-fermion models as their low-energy effective description.

As a generic example, consider a typical realistic spin-fermion model consisting of coupled local moments affected by itinerant carriers [41,42,55–58]:

$$H = \sum_{i \neq i'} J_{ii'} \mathbf{S}_i \cdot \mathbf{S}_{i'} - \frac{J_F}{2} \sum_{imv} \mathbf{S}_i \cdot c_{imv}^\dagger \sigma_{vv'} c_{imv'} + \sum_{jj'mm'v} t_{jmj'm'} c_{jmv}^\dagger c_{j'm'v}, \quad (1)$$

where the local moments  $\mathbf{S}_i$  at site  $i$  and  $i'$  couple via  $J_{ii'}$  such that a magnetic stripe  $(\pi, 0)$  order is preferred by the local moments [41]. The nontrivial physics emerges when these local moments couple to the itinerant carriers  $c_{imv}^\dagger$  of orbital  $m$  and spin  $v$  at the same site  $i$  via coupling constant  $J_F$ , where  $\sigma_{vv'}$  are the Pauli matrices. This is because the itinerant carriers can propagate between sites with kinetic parameter  $t_{jmj'm'}$  and are thus able to mediate an effective long-range interaction [46–48] between the local moments at longer timescale (or lower energy) relevant to the slower spin dynamics. In this general case, the fermion orbitals at sites  $j$  can reside at the same site  $i$  as the local moments or those without (such as ligand sites).

We proceed with the following steps. We first integrate out the influence of the itinerant carriers to second order, which associates their long-range fluctuation with the effective interaction between the local moments. We then demonstrate the system’s failed-order nature using the linear response of the ordered state as a measure of its instability. After that, we simulate the disorder effect numerically and confirm the establishment of long-range order. Finally, we analyze the various emergent length scales in our result and provide an intuitive microscopic picture for the leading physics.

### B. Integrating out itinerant carriers

The emergent magnetic interaction can be obtained by integrating out the faster itinerant electron degrees of freedom. For simplicity, we stick to the weak coupling regime where  $J_F$  can be considered a perturbation that renormalizes [41,42,56] the linear spin-wave theory [59] (also see Appendix A) for the preferred long-range ordered state. Represented in the second quantized magnon creation operator  $a_i^\dagger$  associated with the Holstein-Primakoff transformation [60], the resulting spin-

wave Hamiltonian reads as

$$H^{SW} = \sum_i \tilde{K}_i a_i^\dagger a_i + \sum_{i \neq i'}^{\text{FM}} \tilde{J}_{ii'} (a_i^\dagger a_{i'} + a_i a_{i'}^\dagger) + \sum_{i \neq i'}^{\text{AF}} \tilde{J}_{ii'} (a_i^\dagger a_{i'}^\dagger + a_i a_{i'}), \quad (2)$$

where  $\tilde{K}_i = 2 \sum_{i'}^{\text{AF}} \tilde{J}_{ii'} - 2 \sum_{i'}^{\text{FM}} \tilde{J}_{ii'}$  ensures the preservation of the Goldstone mode of the ordered system. Here for clarity, the summation is split into those between the parallel (FM) and antiparallel (AF) pairs of spins. The effective couplings are renormalized by  $\tilde{J}_{ii'} = J_{ii'} + A_{ii'}$  and  $\tilde{J}_{ii'}^\dagger = J_{ii'} + B_{ii'}$ , respectively, where  $A_{ii'}$  and  $B_{ii'}$  denote the (long-range) magnetic coupling mediated through itinerant carriers.

### C. Failed-order state

We now seek a failed-order state as the unordered state prior to the introduction of chemical or lattice disorder. It was recently suggested [41] that the semimetallic FeSe is such a failed-ordered system whose AFM order only appears under external pressure greater than 1 GPa when the carrier density decreases. In essence, the reduction of carrier density weakens the carrier-induced long-range fluctuation and in turn allows the long-range AFM order of the local moments to emerge. The fact that the failed-order state can be overcome by mere 1 GPa of pressure implies that the long-range fluctuation is close to being overcome by the ordering, making it an ideal model system for our demonstration. We thus take the parameters of Eq. (1) from the previous density-function based study [41], which incorporates  $t_{jmj'm'}$  of five  $d$  orbitals and three  $p$  orbitals,  $J_F = 0.8$  eV,  $S = 1.7$ , and  $J = 19$  and 12 meV for the nearest and next-nearest neighbors, respectively. A discrete  $500 \times 500$  momentum mesh and a 10-meV thermal broadening are used to ensure a good convergence.

Let us first verify the failed-order state before introducing disorder scattering, by examining the stability of the ordered state via its linear response. Figure 2(a) and its inset show that in the absence of disorder, the obtained spin-wave energy-momentum dispersion displays no positive-energy excitation in the vicinity of  $(\pi, 0)$ . Such lack of positive-energy excitation in the linear response is a direct indication that the assumed AFM ordered state is unstable, in this case due to the carrier-induced long-range fluctuation that overwhelms the correlation at length scale longer than  $2\pi/\Delta q$ . In other words, we have verified that our starting point is indeed a failed-order state, in which the local moments are unable to establish long-range order even at the zero-temperature limit [61].

### D. Simulating disorder scattering

We now proceed to include the effect of disorder-induced scattering on the itinerant carriers and investigate its effect on the long-range order. Specifically, we aim to calculate the linear response of the long-range ordered state by ensemble averaging over a large number of chemically disordered configurations. It is well established [46–48] that the main effect of disorder on the magnetic quantum fluctuation of itinerant

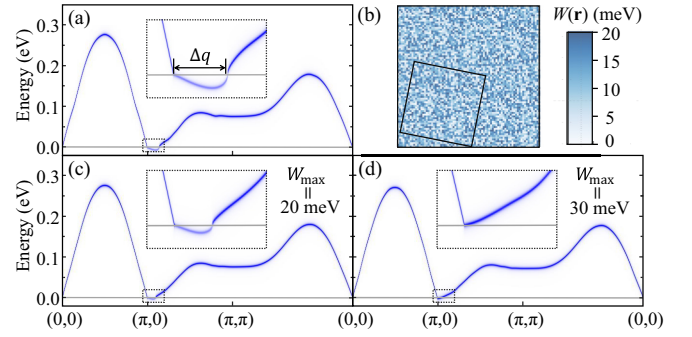


FIG. 2. An example of rekindled failed order. (a) In the failed-order state, imaginary frequency (shown as negative energy) appears near  $(\pi, 0)$  in magnon dispersion as magnified in the inset, indicating that the  $(\pi, 0)$  AFM order is unstable due to carrier-induced fluctuation at long range beyond  $2\pi/\Delta q$ . (b) Illustration of one disorder configuration containing 1664 sites in a  $80 \times 80$  grid, with randomly sampled  $W(\mathbf{r})$  within  $[0, W_{\max}]$ . The orientation of periodicity of each disorder configuration (represented by the tilted square) is randomly chosen to suppress the associated artifacts. (c) Introduction of disorder with strength  $W_{\max} = 20$  meV weakens the long-range fluctuation, allowing the correlation to extend to a longer  $2\pi/\Delta q$  range. (d) By  $W_{\max} = 30$  meV, all excitation energies become real and positive ( $\Delta q = 0$ ), indicating that the preferred magnetic order is a stable phase. In other words, the electronic long-range order is induced upon introduction of weak disorder.

ant carriers is to introduce incoherent phase shifts along its propagation without affecting its power-law spatial decaying profile. We therefore approximate the incoherent phase shifts in the fluctuation within each configuration according to [47]

$$\tilde{J}_{ii'} \longrightarrow \tilde{J}_{ii'} \cos \phi_{ii'}, \quad (3)$$

where

$$\phi_{ii'} = \frac{2}{\hbar v_F} \int_{\mathbf{r}_{i'}}^{\mathbf{r}_i} ds W(\mathbf{r}) \quad (4)$$

accumulates phase shift from scattering against spatially random potential  $W(\mathbf{r})$  along a straight path from position  $\mathbf{r}_{i'}$  of site  $i'$  to position  $\mathbf{r}_i$  of site  $i$  (see the Appendix D for detail on discretization of the disorder strength and its path integration). The strength of the disorder potential  $W(\mathbf{r})$  is randomly sampled from a uniform distribution between 0 and  $W_{\max}$ . We apply Eq. (3) to disorder configurations with large systems (typically containing around 1600 sites) of various shapes and orientations in the simulation [62–65]. [See Fig. 2(b) for an example.] For each configuration containing different phase shifted  $\tilde{J}_{ii'}$  for each pair of  $i$  and  $i'$  [Eq. (4)], the magnon spectral function is then calculated via numerical bosonic Bogoliubov diagonalization [66] (see also Appendix B) of  $H^{SW}$  followed by the unfolding procedure [67] before being averaged over the ensemble.

### E. Rekindled failed order

Figures 2(c) and 2(d) give the resulting magnon energy-momentum dispersion under increasing disorder strength. Since the main effect of disorder is through the phase shift of the carrier-induced long-range fluctuation, the physical

broadening [62–65] in energy and momentum due to the lack of translational symmetry is not apparent. Interestingly, at  $W_{\max} = 20$  meV [Fig. 2(d)] the momentum region without positive frequency reduces to a smaller one, indicating an increase of the length scale in which the ordering persists. Most importantly, at  $W_{\max} = 30$  meV [Fig. 2(d)] the magnon spectrum shows well-defined positive frequency in the entire momentum space, indicating that the proposed stripe  $(\pi, 0)$  AFM order is a stable state of the system! This confirms our proposal (cf. Fig. 1) that by disturbing enough the carrier-induced long-range fluctuation via disorder scattering, a strong electronic order can emerge from the previous failed-order state.

Figure 2 also shows a clear trend about the emergence of long-range order. As the disorder increases,  $\Delta q$  systematically decreases, reflecting the fact that the correlation is able to extend to a longer length scale  $\sim 2\pi/\Delta q$ . Associated with it is the systematical reduction of the strength of the “negative” frequency (representing imaginary frequency) associated with the unstable magnon mode, indicating that the damaging long-range fluctuation systematically becomes weaker. At the point when the strength is no longer able to negate the magnon frequency,  $\Delta q$  becomes zero and the correlation can extend to the system size and establish the long-range order.

#### F. Length scale analysis

To gain further microscopic insight on how disorder scattering produces this unusual effect, notice that according to Eq. (3), the main effect of the scattering is to induce a phase shift proportional to the path integral. Therefore, one would expect the coherence of the renormalization of  $\tilde{J}_{ij}$  to suffer systematically at longer range. Particularly, beyond a characteristic length scale that emerges when the random fluctuation of the phase reaches the order of  $2\pi$ , the power-law tail of the carrier-induced fluctuation should no longer be effective.

To verify this simple intuition, we investigate the effects of finite length scale of the carrier-induced quantum fluctuation and their influence on the magnon dispersion. Specifically, we introduce a finite scattering rate  $2\eta$  in the evaluation of  $A_{ij}$  and  $B_{ij}$  in a clean system (without disorder) to regulate their effective length scales. Figure 3(a) summarizes the resulting magnon dispersion for  $\eta = 1$  to 7 meV. Indeed, the strength of the imaginary frequency becomes weaker systematically as the scattering rate increases, and eventually all magnon frequency becomes positive at  $\eta > 5$  meV, when the long-range order becomes a stable phase. Notice that the momentum region without positive frequency and its associated  $\Delta q$  scale reduces systematically, just like in the above cases with disorder. As expected, in the aspect of allowing the correlation to grow in range and finally reach a long-range order, a reduction in the length scale of carrier propagation leads to a suppression of the long-range fluctuation similar to that caused by the disorder.

Figure 3(b) provides a more quantitative comparison between several relevant length scales in our results. First, notice that in this length-scaled controlled picture, our results display a well-defined  $q^\chi$  at which the magnon dispersion starts to become “negative.” It turns out that its corresponding length scale  $\lambda^\chi = 2\pi/q^\chi$  follows perfectly the length scale of the

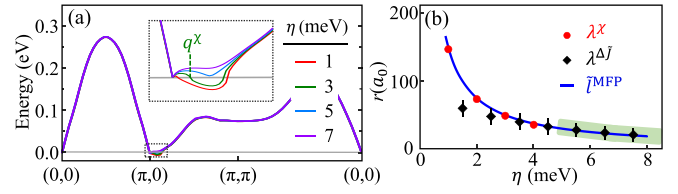


FIG. 3. (a) Magnon energy-momentum dispersion upon restricting the length scale of carrier propagation via controlled scattering rate  $\eta$ . With shorter length scale of coherent propagation (larger scattering rate), the region with imaginary frequency reduced, indicating a longer  $2\pi/\Delta q$  correlation resulting from a shorter length scale  $2\pi/q^\chi$  of the carriers’ damaging fluctuation. By  $\eta > 5$  meV, the excitation energy becomes fully real and positive, so the  $(\pi, 0)$  AFM ordered state becomes stable. (b) In unit of the lattice constant  $a_0$ , the length scale of carrier-induced damaging fluctuation  $\lambda^\chi = 2\pi/q^\chi$  follows perfectly the scale of the mean-free path  $\tilde{l}^{\text{MFP}} \propto v_F/\eta$ . It also roughly corresponds to the length scale of the variation of the emerged long-range coupling  $\lambda^{\Delta J}$ , defined as  $\partial\tilde{J}(r, \eta)/\partial\eta|_{r=\lambda^{\Delta J}} = 0$ . The light green region hosts a stable  $(\pi, 0)$  AFM order.

carrier mean-free path  $\propto v_F/\eta \equiv \tilde{l}^{\text{MFP}}$ . A similar consistency is also found in the length scale of the variation of the emerged long-range coupling (see Appendix E)  $\lambda^{\Delta J}$ , defined through  $\partial\tilde{J}(r, \eta)/\partial\eta|_{r=\lambda^{\Delta J}} = 0$ . In essence, the limitation of the coherent *length scale* of the carrier-induced fluctuation, independent of its origin, leads to a similar suppression of its effectiveness at long range, thereby allowing the correlation to extend to a longer range and eventually establish a long-range order [in the green region in Fig. 3(b)].

#### IV. DISCUSSIONS

Our proposed (purely quantum) mechanism is not to be confused with the quantum adaptation [37,38] of the order-by-disorder effect [33–40] illustrated in Fig. 4(a). In geometric

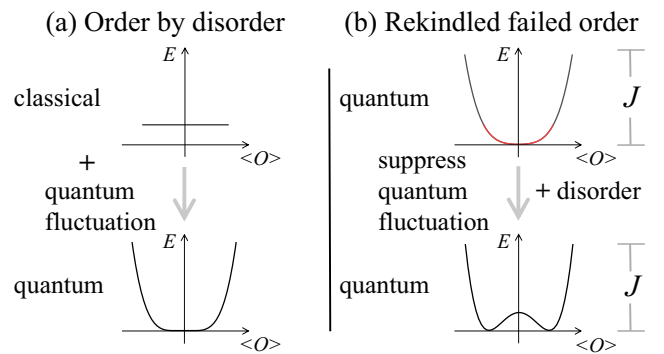


FIG. 4. (a) Illustration of quantum order-by-disorder mechanism vs (b) our rekindled failed-order mechanism. The former starts with heavily degenerate states that get split by quantum fluctuation, while the latter starts with a nondegenerate failed-ordered metallic state that develops degenerate broken-symmetry states upon suppression of long-range fluctuation via disorder scattering. Here  $E$  denotes the typical energy of the system eigenstates with expectation value  $\langle O \rangle$  of the order parameter. Notice that the energy scale of the long-range fluctuation (acting on the red states) can be much weaker than the short-range coupling  $J$ .



frustrated spin systems, classical energy consideration would suggest a heavily degenerate ground-state manifold, with each spin pointing to arbitrary directions. However, as a consequence of the level repulsion principle, quantum fluctuation resulting from coupling within the degenerate manifold can greatly lift the degeneracy to even just a few states. In contrast, our proposal applies to metallic systems with nondegenerate failed-order ground states, as shown in Fig. 4(b). Upon suppression of the long-range fluctuation of itinerant carriers via introduction of chemical or lattice disorder, the ground state becomes degenerate and the system settles in one of the spontaneous broken-symmetry states.

In essence, our proposal uses the disorder-induced decoherence to defeat the long-range fluctuation such that the short-range correlation's tendency toward long-range order can flourish. It is easy to verify (e.g., representative models in the Appendix F) that the above physical effects generally emerge: (a) strong itinerant carrier-induced long-range fluctuation, (b) formation of the failed-order state, and (c) the emergence of long-range order upon suppression of range of coherence of the itinerant carriers. Therefore, our proposal of rekindled failed order, as illustrated in Fig. 1, is completely general, robust, and insensitive to specific models or lattice structures.

Similarly, while the above example concerns only the magnetic order, the underlying principles are generic to almost all symmetry-breaking ordering since they mostly make use of only the general behavior of various mechanisms at long length scales. For example, typical long-range orders are driven by short-range many-body couplings that produce a nonlocal correlation with an exponential decay at a long range. On the other hand, due to the discontinuity associated with the Fermi surface, the fermionic carrier-induced fluctuations usually have a long power-law tail that trumps the exponential decay of the above correlation. This makes our proposed failed order more common than one might realize. Indeed, in strongly correlated materials one often finds a rapid demise of finite-momentum long-range order upon enhancing metallicity, even though the correlations remain very strong at short range. As long as the damaging carrier-induced fluctuation only marginally overwhelms the ordering, our proposed mechanism would apply. By suppressing via weak chemical disorder the carriers' ability to coherently interfere with the ordering at long range, the system has a chance to reveal its preferred long-range electronic order, in magnetic, orbital, charge, or other channels. (Naturally, this mechanism is not expected to apply when disorder becomes so strong that it causes too much damage to the long-range coherence of the ordering itself.)

## V. CONCLUSION

In short, to resolve the long-standing puzzle of the emergence of electronic order via the introduction of chemical disorder widely observed in strongly correlated metals, we propose a rekindled failed-order scenario and verify it through a realistic spin-fermion model and a stability analysis based on linear response of the ordered state. In essence, we propose that many of these strongly correlated metals are in a failed-order state, in which the preferred order of the local moments is overwhelmed by carrier-induced long-range fluctuation.

The main effect of the disorder is to efficiently reduce the coherent length scale of the damaging fluctuation and thereby allow the intrinsic long-range electronic order to emerge. Our study demonstrates a typical example of the rich interplay between mechanisms of multiple length scales present in most strongly correlated metals, to which our proposed simple idea can be applied in general.

## ACKNOWLEDGMENTS

We thank Z. Mao, V. Dobrosavljević, Z.-J. Lang, A. Hegg, F. Gu, and R. Jiang for helpful discussions. This work is supported by the National Natural Science Foundation of China (NSFC) under Grants No. 12274287 and No. 12042507 and the Innovation Program for Quantum Science and Technology Grant No. 2021ZD0301900.

## APPENDIX A: LINEAR SPIN-WAVE THEORY

We review in this Appendix the linear spin-wave theory [59] employed in our analysis for the stability of an ordered state. While the theory is supposed to be accurate only in the well-ordered regime, an unstable response revealed by this theory is still qualitatively indicative to the physical instability.

Start with the Heisenberg Hamiltonian

$$H^{\text{loc}} = \sum_{i \neq i'} J_{ii'} \mathbf{S}_i \cdot \mathbf{S}_{i'}, \quad (\text{A1})$$

where the local moment  $\mathbf{S}_i$  at site  $i$  couple with another spin at site  $i'$  via  $J_{ii'}$  ferromagnetically ( $J_{ii'} < 0$ ) or antiferromagnetically ( $J_{ii'} > 0$ ). If the spins in the system are collinear, it is convenient to transform the spin operators from the local frame to the laboratory frame via a spin rotation

$$S_i^x = \tilde{S}_i^x, \quad S_i^y = \kappa_i \tilde{S}_i^y, \quad S_i^z = \kappa_i \tilde{S}_i^z, \quad (\text{A2})$$

where  $\kappa_i = e^{i\mathbf{Q} \cdot \mathbf{r}_i} = \pm 1$ . The  $x$  and  $y$  components of the spin operator have the relations to the raising operator  $\tilde{S}_i^+$  and lowering operator  $\tilde{S}_i^-$ :

$$\tilde{S}_i^+ = \tilde{S}_i^x + i\tilde{S}_i^y, \quad \tilde{S}_i^- = \tilde{S}_i^x - i\tilde{S}_i^y. \quad (\text{A3})$$

The spin operator can be represented by the bosonic operator via the Holstein-Primakoff (HP) transformation [60] up to the leading order,

$$\tilde{S}_i^z = S - a_i^\dagger a_i, \quad \tilde{S}_i^+ = \sqrt{2S} a_i, \quad \tilde{S}_i^- = \sqrt{2S} a_i^\dagger, \quad (\text{A4})$$

where  $S$  is the magnitude of spin, and  $a_i^\dagger$  is the creation operator. Therefore, we can obtain the quadratic linear spin-wave Hamiltonian with bosonic operators

$$H^{\text{loc}} = \sum_i K_i a_i^\dagger a_i + \sum_{i \neq i'}^{\text{FM}} J_{ii'} (a_i^\dagger a_{i'} + a_i a_{i'}^\dagger) + \sum_{i \neq i''}^{\text{AF}} J_{ii''} (a_i^\dagger a_{i''}^\dagger + a_i a_{i''}), \quad (\text{A5})$$

where  $K_i = 2 \sum_{i''}^{\text{AF}} J_{ii''} - 2 \sum_{i'}^{\text{FM}} J_{ii'}$  ensures preservation of the Goldstone mode of the ordered system. Here the summation is split into those between the parallel (FM) and

antiparallel (AF) pairs of spins. The bosonic operators satisfy the commutation relations

$$[a_i, a_{i'}^\dagger] = \delta_{ii'}, \quad [a_i^\dagger, a_i^\dagger] = [a_i, a_{i'}] = 0. \quad (\text{A6})$$

A simple one-band spin-wave Hamiltonian represented in momentum  $q$  space is

$$H^{\text{loc}} = \sum_q J^A(q)(a_q^\dagger a_q + a_{-q} a_{-q}^\dagger) + J^B(q)(a_q^\dagger a_{-q}^\dagger + a_q a_{-q}), \quad (\text{A7})$$

where  $J^A(q)$  is the coefficient after Fourier transformation of  $a_i^\dagger a_{i'}$  ( $i = i'$  or  $i \neq i'$ ) and  $J^B(q)$  is the coefficient after Fourier transformation of  $a_i^\dagger a_{i'}^\dagger$ . The corresponding spin-wave dispersion is

$$\omega(q) = \sqrt{[J^A(q)]^2 - [J^B(q)]^2}. \quad (\text{A8})$$

## APPENDIX B: BOGOLIUBOV DIAGONALIZATION OF GENERAL QUADRATIC BOSONIC HAMILTONIAN

This Appendix introduces a method to diagonalize a general Bogoliubov Hamiltonian beyond the standard  $2 \times 2$  size, following the previous proposal [66]. Considering a general quadratic bosonic Hamiltonian

$$H = \sum_{ij} t_{ij} a_i^\dagger a_j + \tau_{ij} a_i^\dagger a_j^\dagger + \tau_{ij}^* a_i a_j, \quad (\text{B1})$$

where  $t_{ij}$  is the hopping parameter, and  $\tau_{ij}$  is the parameter for creating two bosons with index  $i$  and  $j$ . Since Hamiltonian is Hermitian,  $t_{ij} = t_{ji}^*$  and  $\tau_{ij} = \tau_{ji}$ . The Hamiltonian represented in the diagonal basis is

$$H = \sum_i \epsilon_i b_i^\dagger b_i, \quad (\text{B2})$$

where  $\epsilon_i$  is the eigenvalues of index  $i$ . The new bosonic operators  $b_i^\dagger$  satisfy the bosonic commutation relations that same as  $a_i^\dagger$  in Eq. (A6). There are relations between the new and old bosonic operators,

$$b_i^\dagger = \sum_j a_j^\dagger T_{ji}^N + \sum_j a_j T_{ji}^A, \quad b_i = \sum_j a_j T_{ji}^{N*} + \sum_j a_j^\dagger T_{ji}^{A*}, \quad (\text{B3})$$

where  $T_{ji}^N$  and  $T_{ji}^A$  are the eigenvectors. Therefore, we can define a redundant and overcomplete basis:

$$A_I^\dagger = \begin{cases} a_i^\dagger, & I \in U \\ a_i \ (i = I - \text{No. of } i), & I \in D \end{cases}, \quad B_I^\dagger = \sum_j A_j^\dagger T_{JI}, \quad (\text{B4})$$

where  $U$  and  $D$  mean the up and down channel, respectively.  $T_{JI}$  is the matrix of eigenvectors

$$T_{JI} \longrightarrow \begin{pmatrix} T_{ji}^N & T_{ji}^{A*} \\ T_{ji}^A & T_{ji}^{N*} \end{pmatrix}. \quad (\text{B5})$$

Due to the bosonic commutation relations, there is

$$[B_I, B_J^\dagger] = c_I \delta_{IJ}, \quad \text{where } c_I = \begin{cases} 1, & I \in U \\ -1, & I \in D. \end{cases} \quad (\text{B6})$$

Substituting Eq. (B4) into (B6), we can obtain the rule of orthonormalizing eigenvectors

$$\sum_{I'J'} [A_{I'}, A_{J'}^\dagger] T_{I'I}^* T_{J'J} = \sum_K c_K T_{KI}^* T_{KJ} = c_I \delta_{IJ}. \quad (\text{B7})$$

The commutating result between Hamiltonian and  $B_I^\dagger$  is

$$[H, B_I^\dagger] = c_I \epsilon_I B_I^\dagger = \sum_J A_J^\dagger T_{JI} c_I \epsilon_I. \quad (\text{B8})$$

Equation (B8) also can be expressed using Eq. (B4) as

$$\begin{aligned} \sum_K [H, A_K^\dagger] T_{KI} &= \sum_{k \in U} \left( \sum_j t_{jk} a_j^\dagger + \sum_j (\tau_{kj}^* + \tau_{jk}^*) a_j \right) T_{KI} \\ &\quad - \sum_{k \in D} \left( \sum_j t_{kj} a_j + \sum_j (\tau_{kj} + \tau_{jk}) a_j^\dagger \right) T_{KI}. \end{aligned} \quad (\text{B9})$$

Combining Eqs. (B8) and (B9), we find

$$T_{JI} c_I \epsilon_I = \sum_K M_{JK} T_{KI}, \quad (\text{B10})$$

where

$$M_{JK} = \begin{pmatrix} t_{jk} & -2\tau_{jk} \\ 2\tau_{jk}^* & -t_{kj} \end{pmatrix}. \quad (\text{B11})$$

The non-Hermitian matrix  $M$  is the matrix that we should diagonalize, and we can derive the eigenvalues  $\epsilon_I$  and corresponding eigenvectors by solving  $M$ .

## APPENDIX C: INTEGRATING OUT THE CARRIERS

Here, we derive the effective linear spin-wave Hamiltonian via integrating out the influence of itinerant carriers [41,42,56]. In general, the spin-fermion Hamiltonian contains local moments and itinerant carriers

$$H = H^{\text{loc}} + H^{\text{it}} + H^{\text{F}}, \quad (\text{C1})$$

where  $H^{\text{loc}}$  is the spin Hamiltonian of local moments,  $H^{\text{it}}$  is the Hamiltonian of itinerant carriers, and  $H^{\text{F}}$  describes the coupling between local moments and itinerant carriers. For simplicity,  $H^{\text{F}}$  is Hund's coupling-like, and we use the one-band linear spin-wave Hamiltonian in Eq. (A7) as an example to show how to integrate out the itinerant carriers.

We treat the Hund's coupling  $J_{\text{F}}$  between the itinerant and local degrees of freedom as perturbation

$$H^{\text{F}} = -\frac{J_{\text{F}}}{2} \sum_{imv\nu'} \mathbf{S}_i c_{imv}^\dagger \boldsymbol{\sigma}_{\nu\nu'} c_{imv}, \quad (\text{C2})$$

where  $\boldsymbol{\sigma}_{\nu\nu'}$  are the Pauli matrices and  $c_{imv}^\dagger$  represents creating an itinerant carrier at site  $i$  of orbital  $m$  with spin  $\nu$ . Applying a canonical transformation to the Hamiltonian in Eq. (C1),

$$e^\Lambda H e^{-\Lambda} = H + [\Delta, H] + \frac{1}{2}[\Delta, [\Delta, H]] + \dots, \quad (\text{C3})$$

results in the renormalized linear spin-wave Hamiltonian from its quadratic components

$$\begin{aligned} H^{\text{SW}} &= H^{\text{loc}} + \langle (H^{\text{F}})^2 + \frac{1}{2}[\Delta, (H^{\text{F}})^{(1)}] \rangle_e \\ &= \sum_q [\tilde{J}^{\text{A}}(q)(a_q^\dagger a_q + a_{-q}^\dagger a_{-q}) + \tilde{J}^{\text{B}}(q)(a_q^\dagger a_{-q}^\dagger + a_{-q} a_q)] \end{aligned} \quad (\text{C4})$$

up to the second order of bosonic operators, where

$$\tilde{J}^{\text{A}}(q) = J^{\text{A}}(q) + A(q), \quad \tilde{J}^{\text{B}}(q) = J^{\text{B}}(q) + B(q). \quad (\text{C5})$$

Here,

$$A(q) = \frac{J_{\text{F}}^2 S}{2N} \sum_{kl'l'} \frac{f_l(k) - f_{l'}(k+q)}{E_l(k) - E_{l'}(k+q)} \left| \sum_m U_{m\downarrow}^{l'\star}(k+q) U_{m\uparrow}^l(k) \right|^2 \quad (\text{C6})$$

and

$$\begin{aligned} B(q) &= \frac{J_{\text{F}}^2 S}{2N} \sum_{kl'l'} \frac{f_l(k) - f_{l'}(k+q)}{E_l(k) - E_{l'}(k+q)} \\ &\quad \times \sum_{mm'} U_{m\downarrow}^{l'\star}(k+q) U_{m\uparrow}^l(k) U_{m'\downarrow}^{l'\star}(k) U_{m'\uparrow}^l(k+q), \end{aligned} \quad (\text{C7})$$

where  $E_l(k)$  denotes the eigenvalues with momentum  $k$  and band index  $l$  (that absorbs the spin index as well) and  $U_{mv}^l(k)$  denotes the eigenvectors in the basis of orbital  $m$  with spin  $v = \uparrow$  or  $\downarrow$ .  $N$  denotes the number of discrete momenta of the system.  $f_l(k) = \frac{1}{1 + e^{\beta(E_l(k) - \mu)}}$  is the standard Fermi-Dirac distribution function for a given chemical potential  $\mu$ , and  $S$  the effective magnitude of the local moments. Note that  $J^{\text{A}}(q)$  contains the a constant correction term  $\frac{J_{\text{F}}}{2N} \sum_{kl} f_l(k) \sum_{mv} v |U_{mv}^l(k)|^2$  that is from the Hund's coupling.

We also can get similar results using a dynamic method by using the perturbation theory with Green's function to integrate out the carrier channel. The real part of the susceptibility in momentum  $q$  space is

$$\begin{aligned} A(q) &= \frac{J_{\text{F}}^2 S}{2N} \sum_{kl'l'} \frac{[f_l(k) - f_{l'}(k+q)][E_l(k) - E_{l'}(k+q)]}{[E_l(k) - E_{l'}(k+q)]^2 + \delta^2} \\ &\quad \times \left| \sum_m U_{m\downarrow}^{l'\star}(k+q) U_{m\uparrow}^l(k) \right|^2 \end{aligned} \quad (\text{C8})$$

and

$$\begin{aligned} B(q) &= \frac{J_{\text{F}}^2 S}{2N} \sum_{kl'l'} \frac{[f_l(k) - f_{l'}(k+q)][E_l(k) - E_{l'}(k+q)]}{[E_l(k) - E_{l'}(k+q)]^2 + \delta^2} \\ &\quad \times \sum_{mm'} U_{m\downarrow}^{l'\star}(k+q) U_{m\uparrow}^l(k) U_{m'\downarrow}^{l'\star}(k) U_{m'\uparrow}^l(k+q). \end{aligned} \quad (\text{C9})$$

The typical numerical broadening of  $\delta = 0^+$  is not necessary here since we are only interested in the zero-frequency limit of the renormalization. We can investigate the effects of the finite length scale of the carrier propagation on their quantum fluctuation and in turn the influence on the magnon dispersion. This is easily implemented by imposing a finite one-body scattering rate  $\eta$  in Eq. (C8) via  $\delta = 2\eta$ . Diagonalization of

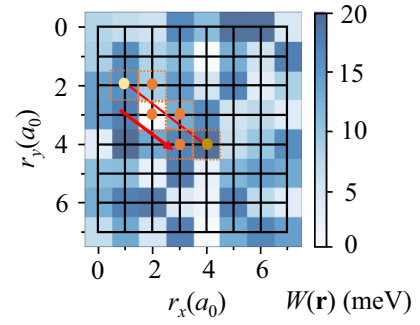


FIG. 5. An example path integral of the disorder-dependent phase factor in a discrete  $8 \times 8$  lattice from light yellow site (1,2) to dark yellow site (4,4). Along the straight path, it would pass a set of squares with different depths of blue color which represent the strength of potential energy  $W(\mathbf{r})$ .

the spin-wave Hamiltonian gives the spin-wave dispersion

$$\omega(q) = \sqrt{[\tilde{J}^{\text{A}}(q)]^2 - [\tilde{J}^{\text{B}}(q)]^2}. \quad (\text{C10})$$

#### APPENDIX D: WEAK DISORDER ON THE EMERGED LONG-RANGE COUPLINGS

Here, we will show the procedure of introducing the weak effect of charge disorder on the emerged long-range couplings. It is well known [46–48] that the main effect of disorder-induced scattering on the magnetic quantum fluctuation of itinerant carriers is to introduce incoherent phase shifts along its propagation without affecting its power-law spatial decaying profile. When the Fermi wave vector  $\mathbf{k}_{\text{F}}$  is well defined, the oscillations with weak nonmagnetic disorders can be expressed as [47]  $J(\mathbf{r}) \cos(2\mathbf{k}_{\text{F}} \cdot \mathbf{r} + \phi_{\mathbf{r}})$ , where  $J(\mathbf{r})$  is the magnitude with power-law decaying,  $\mathbf{r}$  is the vector different between different positions in real space. In discrete lattice, the renormalized linear spin-wave Hamiltonian in Eq. (C4) can be represented in real space in terms of Eq. (A5) via Fourier transformation with renormalized spin-spin coupling parameter  $\tilde{J}_{i'i'}$ . The renormalized spin-spin coupling parameter contains the oscillating factor  $\cos[2\mathbf{k}_{\text{F}}(\mathbf{r}_i - \mathbf{r}_{i'})]$  between different sites. However, in realistic systems, the Fermi surface is typically not perfectly nested and thus the oscillation in  $\tilde{J}_{i'i'}$  is not with a fixed  $2\mathbf{k}_{\text{F}}$  period, but instead, it displays a rather complicated pattern. We therefore approximate the disorder-induced phase shift via

$$\tilde{J}_{i'i'} \longrightarrow \tilde{J}_{i'i'} \cos \phi_{i'i'}, \quad (\text{D1})$$

where  $\tilde{J}_{i'i'}$  contains the power-law decaying term and oscillating term. The disorder-dependent phase is

$$\phi_{i'i'} = \frac{2}{\hbar v_{\text{F}}} \int_{\mathbf{r}_i}^{\mathbf{r}_{i'}} ds W(\mathbf{r}), \quad (\text{D2})$$

where  $W(\mathbf{r})$  denotes the strength of the spatial disorder randomly sampled from a uniform distribution between 0 and  $W_{\text{max}}$  and the integration is along a straight path from position  $\mathbf{r}_i$  of site  $i$  to position  $\mathbf{r}_{i'}$  of site  $i'$ . Here  $v_{\text{F}}$  is the Fermi velocity and  $\hbar$  is 1 in the atomic unit. The Fermi velocity in our calculation is estimated via the derivative of the Hamiltonian concerning its momentum around Fermi energy. Then we will show how to discretize the disorder-dependent phase factor from a continuum space to a discrete lattice. An example of

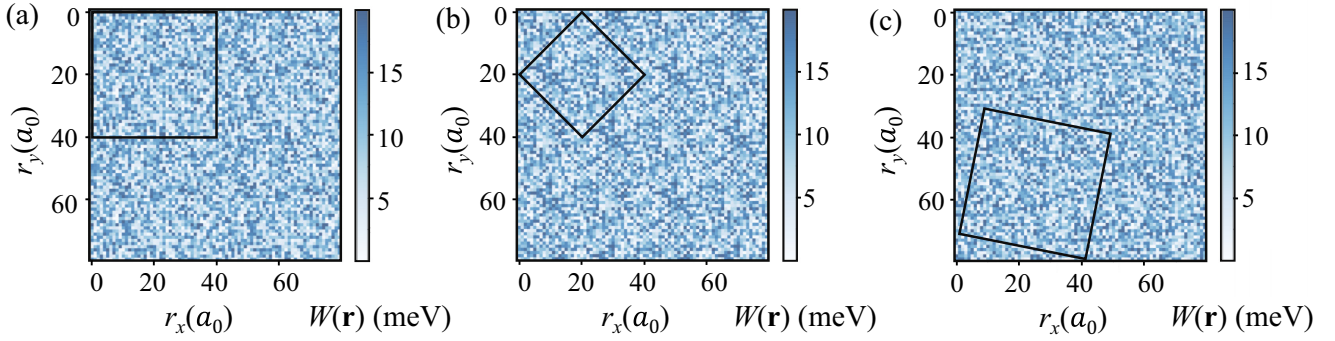


FIG. 6. Examples of disorder configurations with the maximum value  $W_{\max} = 20$  meV in an  $80 \times 80$  lattice. The black dotted squares show disordered patterns which have different sizes and orientations.

discretizing the phase factor is shown as Fig. 5. Every site at the lattice has different random potential energy from zero to a maximum potential energy  $W_{\max}$ . We treat the potential energy  $W(\mathbf{r})$  dominating a square range around the site  $\mathbf{r}_i$ . The total phase factor is the summation of  $W(\mathbf{r}) \times ds$  from  $\mathbf{r}_i$  to  $\mathbf{r}_j$ .  $ds$  is the length in the square range around the disorder site. We generate random potential  $\mathbf{r}_i$  in lattice with different sizes and orientations in the range of  $[0, W_{\max}]$ . Three kinds of disorder configurations as examples are shown in Fig. 6.

#### APPENDIX E: LENGTH SCALE OF VARIATION OF THE EMERGED LONG-RANGE COUPLING

As discussed in Appendix C, the resulting renormalized spin-wave Hamiltonian is in Eq. (C4) with the coefficients  $\tilde{J}^A$  and  $\tilde{J}^B$  including  $A(q)$  in Eq. (C8) and  $B(q)$  in Eq. (C9), respectively. These coefficients become different with different scattering rates  $\eta$ , resulting in different long-range couplings  $\tilde{J}_{ij}$  in real space.

The dispersion of the pure FeSe in Fig. 2(a) shows the magnetic order is unstable along the  $q_y$  direction. Therefore, we can summate the contributions of  $\tilde{J}_{ij}$  along the  $x$  direction and obtain the fluctuating decaying couplings along the  $y$  direction.

Figure 7 shows the renormalized spin-spin interaction  $\tilde{J}$  at long distances with different  $\eta = 1$  and 7 meV for FeSe as an example. The coupling is suppressed at long range

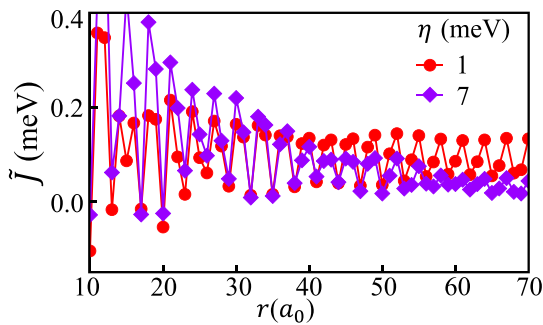


FIG. 7. Renormalized spin-spin interaction  $\tilde{J}$  along  $y$  direction at the range from  $10a_0$  to  $70a_0$  with scattering rate 1 and 7 meV.  $\tilde{J}$  is oscillating decaying. The two different lines across this range that show the long-range coupling is suppressed when the disorder is stronger.

and enhanced at short range with increasing damping energy. Since lines with different  $\eta$  would cross with each other, we can define a length scale  $\lambda^{\Delta J}$  as  $\partial \tilde{J}(r, \eta) / \partial \eta|_{r=\lambda^{\Delta J}} = 0$ . Such a length scale can be estimated from the plot with an error bar.

#### APPENDIX F: MORE DEMONSTRATION OF THE REKINDLED FAILED-ORDER MECHANISM

To verify the general “rekindled failed-order” mechanism, we provide here two more rather generic examples: (1) a one-band model on a square lattice with local spin-fermion coupling, and (2) a decorated square lattice with nonlocal spin-fermion coupling, to demonstrate the generality of our proposal. All the examples display similar (a) strong itinerant carrier-induced long-range fluctuation, (b) formation of the failed-order state, and (c) the emergence of long-range order upon suppression of the range of coherence of the itinerant carriers, as the robust consequence of the underlying generic physical effect mentioned in the paper. Example (1) can be viewed as the example of one-band spin-fermion model, and (2) is similar to the cuprate system that belongs to doped charge transfer insulators.

##### 1. One-band spin-fermion model

We construct a translational symmetric two-dimensional one-band Hamiltonian for the itinerant carriers with the nearest neighboring  $t = -0.2$  eV by treating the out-of-plane terms small. Here, we choose the filling factor 0.9 near the half-filling case. The Neel AFM state is the reference magnetic ordered state with the parameter  $J = 2$  meV for the nearest neighbors of the local moments for  $S = 1$ . The Hamiltonian of the coupling between the local moments and the itinerant carriers is the same with Eq. (C2), and the parameter is  $J_F = 0.6$  eV. We use the method mentioned above in Appendix C to integrate out the carriers and obtain the magnetic susceptibility of a failed-order state shown in Fig. 8(a). A discrete  $500 \times 500$  momentum mesh and a 100-meV thermal broadening are used to ensure a good convergence.

As shown in Fig. 8(a), the obtained magnetic susceptibility displays no positive-energy excitation in the vicinity of  $(\pi, \pi)$  and  $(0,0)$  indicating the assumed AFM ordered state is unstable. Since the carrier-induced long-range fluctuation overwhelms the correlation at long range, the local moments are unstable to establish long-range order at zero-temperature



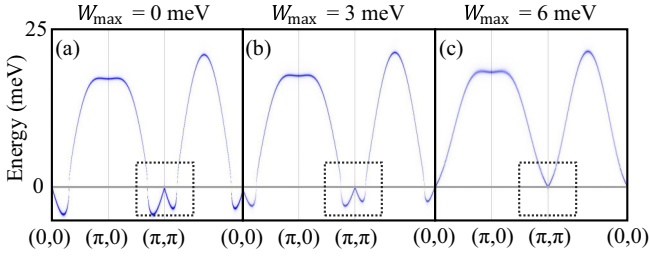


FIG. 8. Emergence of long-range magnetic order via the introduction of disorder to a failed-ordered metal with large magnetic moments. Magnetic susceptibility is shown here as a measure of the stability of the preferred ordered state. (a) In the clean system ( $W_{\max} = 0$ ) imaginary (shown as negative) frequency appears near  $(\pi, \pi)$  and  $(0,0)$ , indicating the  $(\pi, \pi)$  AFM order is unstable due to carrier-induced fluctuation at long range. (b) Introduction of disorder with  $W_{\max} = 3$  meV weakens the fluctuation, allowing the correlation to extend to a longer range. (c) By  $W_{\max} = 6$  meV, all excitation energies become positive, indicating the correlation is now long range and the preferred  $(\pi, \pi)$  magnetic order is a stable phase. That is, the electronic long-range order is induced by the introduction of chemical disorder.

limit. When increasing disorder strength, for example at  $W_{\max} = 3$  meV [Fig. 8(b)], the momentum region without positive frequency is reduced which indicates an increase of the ordering length scale. At  $W_{\max} = 6$  meV [Fig. 8(c)], the magnon spectrum shows well-defined positive frequency in the entire momentum space, indicating that the proposed Neel  $(\pi, \pi)$  AFM order is a stable state of the system!

## 2. Doped charge transfer insulator

For doped charge transfer insulators like cuprate, an effective spin-fermion model can be derived from a multiband Hubbard model via integrating out the high-energy physics [52]. The effective spin-fermion model in cuprates contains two different orbitals for itinerant carriers residing on O and the local spins at Cu. Different from the previous examples mentioned above, the couplings between itinerant carriers and local moments are nonlocal. For simplicity, we consider the coupling between local moments and itinerant carriers as

$$H^F = \frac{J_F}{2} \sum_{ijm\nu\nu'} S_i \cdot c_{jmv}^\dagger \sigma_{\nu\nu'} c_{jmv'}, \quad (\text{F1})$$

where the local moments are at the copper site  $i$  and itinerant carriers are located at the oxygen  $j$ . In this case, the carriers are not renormalized by the AFM order state if the spins lack quantum fluctuations.

Using the same method discussed in Appendix C, we can derive the itinerant carrier-induced spin-spin couplings in real space:

$$J_{0i}^F = \frac{2J_F^2}{N} \sum_{i, \mathbf{k}_1, \mathbf{k}_2, l, l'} \cos[\mathbf{r}_i(\mathbf{k}_1 - \mathbf{k}_2)] \frac{f_l(\mathbf{k}_2) - f_l(\mathbf{k}_1)}{E_l(\mathbf{k}_2) - E_l(\mathbf{k}_1)} \times \left| \sum_m \cos\left(\frac{k_{1,m} - k_{2,m}}{2}\right) U_{m,\uparrow}^{l'\star}(\mathbf{k}_1) U_{m,\downarrow}^l(\mathbf{k}_2) \right|^2, \quad (\text{F2})$$

where  $N$  denotes the number of discrete momenta of the system. When  $m = 1$  or  $2$ , the momentum  $\mathbf{k}$  only

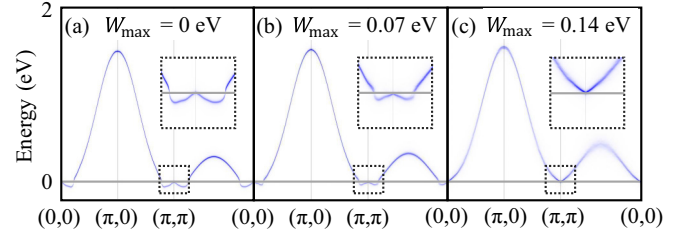


FIG. 9. Emergence of long-range magnetic order via the introduction of disorder to a failed-ordered metal with large magnetic moments. Magnetic susceptibility is shown here as a measure of the stability of the preferred ordered state. (a) In the clean system ( $W_{\max} = 0$ ) imaginary (shown as negative) frequency appears near  $(\pi, \pi)$  and  $(0,0)$ , indicating the  $(\pi, \pi)$  AFM order is unstable due to carrier-induced fluctuation at long range. (b) Introduction of disorder with  $W_{\max} = 0.07$  eV weakens the fluctuation, allowing the correlation to extend to a longer range. (c) By  $W_{\max} = 0.14$  eV, all excitation energies become positive, indicating the correlation is now long range and the preferred  $(\pi, \pi)$  magnetic order is a stable phase.

have the  $x$  or  $y$  component. The total contribution  $\tilde{J}_{0i}$  contains the bare coupling of the local moments  $J_{0i}$  and the long-range fluctuations  $J_{0i}^F$ .

Having these necessary methods, we construct a translational symmetric two-dimensional two-band cupratelike Hamiltonian for the itinerant carriers with the nearest-neighboring hopping  $|t_1| = 1$  eV and the next-nearest-neighboring hopping  $|t_2| = 0.8$  eV by treating the out-of-plane terms small. 15% hole doping is chosen in this case. The AFM ordered state with parameters  $J = 0.93$  eV for the nearest neighbors of the local moments. The AFM coupling between local moments and itinerant carriers is  $J_F = 0.5$  eV. The magnitude of spin is  $S = 1$ . A discrete  $300 \times 300$  momentum mesh and a 100-meV thermal broadening are used to ensure a good convergence. Using the methods including integrating out the carriers, linear spin-wave theory, and the introduction of disorder mentioned above, we can obtain the magnetic susceptibility with and without disorder.

As shown in Fig. 9(a), the obtained magnetic susceptibility displays no positive-energy excitation in the vicinity of  $(\pi, \pi)$  and  $(0,0)$  indicating the assumed AFM ordered state is unstable. Since the carrier-induced long-range fluctuation overwhelms the correlation at long range, the local moments are unstable to establish long-range order at zero-temperature limit. When increasing disorder strength, for example at  $W_{\max} = 0.07$  eV [Fig. 9(b)], the momentum region without positive frequency is reduced which indicates an increase of the ordering length scale. At  $W_{\max} = 0.14$  eV [Fig. 9(c)], the magnon spectrum shows well-defined positive frequency in the entire momentum space, indicating that the proposed Neel  $(\pi, \pi)$  AFM order is a stable state of the system!

In reality, the indications that AFM order could emerge from unordered systems also have been found in hole-doped cuprates via Zn substitution of Cu, as measured by muon spin resonance ( $\mu$ SR) [21] and neutron scattering experiments [20,22,23]. A strong electronic order can emerge from the failed-order state via the introduction of disorder, and the results are generic.

- [1] L. Shen, C. Greaves, R. Riyat, T. C. Hansen, and E. Blackburn, Absence of magnetic long-range order in  $\text{Y}_2\text{CrSbO}_7$ : Bond-disorder-induced magnetic frustration in a ferromagnetic pyrochlore, *Phys. Rev. B* **96**, 094438 (2017).
- [2] S.-W. Cheong, A. S. Cooper, L. W. Rupp, B. Batlogg, J. D. Thompson, and Z. Fisk, Magnetic dilution study in  $\text{La}_2\text{CuO}_4$ : Comparison with other two-dimensional magnets, *Phys. Rev. B* **44**, 9739 (1991).
- [3] O. P. Vajk, P. K. Mang, M. Greven, P. M. Gehring, and J. W. Lynn, Quantum impurities in the two-dimensional spin one-half Heisenberg antiferromagnet, *Science* **295**, 1691 (2002).
- [4] J.-Y. P. Delannoy, A. G. Del Maestro, M. J. P. Gingras, and P. C. W. Holdsworth, Site dilution in the half-filled one-band Hubbard model: Ring exchange, charge fluctuations, and application to  $\text{La}_2\text{Cu}_{1-x}(\text{Mg}/\text{Zn})_x\text{O}_4$ , *Phys. Rev. B* **79**, 224414 (2009).
- [5] R. Schneider, A. G. Zaitsev, D. Fuchs, and H. v. Löhneysen, Superconductor-insulator quantum phase transition in disordered FeSe thin films, *Phys. Rev. Lett.* **108**, 257003 (2012).
- [6] A. P. Mackenzie, R. K. W. Haselwimmer, A. W. Tyler, G. G. Lonzarich, Y. Mori, S. Nishizaki, and Y. Maeno, Extremely strong dependence of superconductivity on disorder in  $\text{Sr}_2\text{RuO}_4$ , *Phys. Rev. Lett.* **80**, 161 (1998).
- [7] K. Fujita, T. Noda, K. M. Kojima, H. Eisaki, and S. Uchida, Effect of disorder outside the  $\text{CuO}_2$  planes on  $T_c$  of copper oxide superconductors, *Phys. Rev. Lett.* **95**, 097006 (2005).
- [8] L. Sham and B. R. Patton, Effect of impurity on a Peierls transition, *Phys. Rev. B* **13**, 3151 (1976).
- [9] J. A. W. Straquadine, F. Weber, S. Rosenkranz, A. H. Said, and I. R. Fisher, Suppression of charge density wave order by disorder in Pd-intercalated  $\text{ErTe}_3$ , *Phys. Rev. B* **99**, 235138 (2019).
- [10] A. Fang, J. A. W. Straquadine, I. R. Fisher, S. A. Kivelson, and A. Kapitulnik, Disorder-induced suppression of charge density wave order: STM study of Pd-intercalated  $\text{ErTe}_3$ , *Phys. Rev. B* **100**, 235446 (2019).
- [11] A. Fang, A. G. Singh, J. A. W. Straquadine, I. R. Fisher, S. A. Kivelson, and A. Kapitulnik, Robust superconductivity intertwined with charge density wave and disorder in Pd-intercalated  $\text{ErTe}_3$ , *Phys. Rev. Res.* **2**, 043221 (2020).
- [12] M. Braden, O. Friedt, Y. Sidis, P. Bourges, M. Minakata, and Y. Maeno, Incommensurate magnetic ordering in  $\text{Sr}_2\text{Ru}_{1-x}\text{Ti}_x\text{O}_4$ , *Phys. Rev. Lett.* **88**, 197002 (2002).
- [13] M. Minakata and Y. Maeno, Magnetic ordering in  $\text{Sr}_2\text{RuO}_4$  induced by nonmagnetic impurities, *Phys. Rev. B* **63**, 180504(R) (2001).
- [14] K. Ishida, Y. Minami, Y. Kitaoka, S. Nakatsuji, N. Kikugawa, and Y. Maeno, Evolution of normal-state magnetic fluctuations by Ca and Ti substitutions in  $\text{Sr}_2\text{RuO}_4$ :  $^{87}\text{Sr}$  - NMR study, *Phys. Rev. B* **67**, 214412 (2003).
- [15] K. Pucher, J. Hemberger, F. Mayr, V. Fritsch, A. Loidl, E.-W. Scheidt, S. Klimm, R. Horny, S. Horn, S. G. Ebbinghaus, A. Reller, and R. J. Cava, Transport, magnetic, thermodynamic, and optical properties in Ti-doped  $\text{Sr}_2\text{RuO}_4$ , *Phys. Rev. B* **65**, 104523 (2002).
- [16] S. Kitagawa, T. Iye, Y. Nakai, K. Ishida, C. Wang, G.-H. Cao, and Z.-A. Xu, Relationship between superconductivity and antiferromagnetism in  $\text{LaFe}(\text{As}_{1-x}\text{P}_x)\text{O}$  revealed by 31P-NMR, *J. Phys. Soc. Jpn.* **83**, 023707 (2014).
- [17] K. T. Lai, A. Takemori, S. Miyasaka, F. Engetsu, H. Mukuda, and S. Tajima, Evolution of the phase diagram of  $\text{LaFeP}_{1-x}\text{As}_x\text{O}_{1-y}\text{F}_y$  ( $y = 0 - 0.1$ ), *Phys. Rev. B* **90**, 064504 (2014).
- [18] H. Mukuda, F. Engetsu, T. Shiota, K. T. Lai, M. Yashima, Y. Kitaoka, S. Miyasaka, and S. Tajima, Emergence of novel antiferromagnetic order intervening between two superconducting phases in  $\text{LaFe}(\text{As}_{1-x}\text{P}_x)\text{O}$ : 31 P-NMR studies, *J. Phys. Soc. Jpn.* **83**, 083702 (2014).
- [19] M. Hücker, V. Kataev, J. Pommer, J. Harraß, A. Hosni, C. Pflichtsch, R. Gross, and B. Büchner, Mobility of holes and suppression of antiferromagnetic order in  $\text{La}_{2-x}\text{Sr}_x\text{CuO}_4$ , *Phys. Rev. B* **59**, R725(R) (1999).
- [20] K. Hirota, K. Yamada, I. Tanaka, and H. Kojima, Quasi-elastic incommensurate peaks in  $\text{La}_{2-x}\text{Sr}_x\text{Cu}_{1-y}\text{Zn}_y\text{O}_{4-\delta}$ , *Phys. B Condensed Matter* **241-243**, 817 (1997), Proceedings of the International Conference on Neutron Scattering.
- [21] I. Watanabe, M. Aoyama, M. Akoshima, T. Kawamata, T. Adachi, Y. Koike, S. Ohira, W. Higemoto, and K. Nagamine, Possibility of an ordered state of spins and holes in single-crystal  $\text{La}_{2-x}\text{Sr}_x\text{Cu}_{1-y}\text{Zn}_y\text{O}_4$  ( $x = 0.21$ ,  $y = 0$  and  $0.01$ ) studied by  $\mu\text{SR}$ , *Phys. Rev. B* **62**, R11985 (2000).
- [22] H. Kimura, M. Kofu, Y. Matsumoto, and K. Hirota, Novel in-gap spin state in Zn-doped  $\text{La}_{1.85}\text{Sr}_{0.15}\text{CuO}_4$ , *Phys. Rev. Lett.* **91**, 067002 (2003).
- [23] A. Suchanek, V. Hinkov, D. Haug, L. Schulz, C. Bernhard, A. Ivanov, K. Hradil, C. T. Lin, P. Bourges, B. Keimer, and Y. Sidis, Incommensurate magnetic order and dynamics induced by spinless impurities in  $\text{YBa}_2\text{Cu}_3\text{O}_{6.6}$ , *Phys. Rev. Lett.* **105**, 037207 (2010).
- [24] Risdiana, T. Saragi, W. A. Somantri, S. Pratiwi, D. Suhendardar, M. Manawan, B. J. Suroto, and I. Watanabe, Zn-induced development of the Cu-spin correlation in electron-doped superconducting cuprates of  $\text{Eu}_{2-x}\text{Ce}_x\text{CuO}_4$ , *J. Phys.: Conf. Ser.* **1013**, 012180 (2018).
- [25] W. Higemoto, M. Yokoyama, T. U. Ito, T. Suzuki, S. Raymond, and Y. Yanase, Direct measurement of the evolution of magnetism and superconductivity toward the quantum critical point, *Proc. Natl. Acad. Sci. USA* **119**, e2209549119 (2022).
- [26] S. Wessel, B. Normand, M. Sigrist, and S. Haas, Order by disorder from nonmagnetic impurities in a two-dimensional quantum spin liquid, *Phys. Rev. Lett.* **86**, 1086 (2001).
- [27] C. Yasuda, S. Todo, M. Matsumoto, and H. Takayama, Site-dilution-induced antiferromagnetic long-range order in a two-dimensional spin-gapped Heisenberg antiferromagnet, *Phys. Rev. B* **64**, 092405 (2001).
- [28] J. Bobroff, N. Lafflorencie, L. K. Alexander, A. V. Mahajan, B. Koteswararao, and P. Mendels, Impurity-induced magnetic order in low-dimensional spin-gapped materials, *Phys. Rev. Lett.* **103**, 047201 (2009).
- [29] J. H. J. Martiny, A. Kreisel, and B. M. Andersen, Theoretical study of impurity-induced magnetism in FeSe, *Phys. Rev. B* **99**, 014509 (2019).
- [30] M. N. Gastiasoro and B. M. Andersen, Local magnetization nucleated by non-magnetic impurities in Fe-based superconductors, *J. Supercond. Novel Magn.* **28**, 1321 (2015).
- [31] B. Zinkl and M. Sigrist, Impurity-induced magnetic ordering in  $\text{Sr}_2\text{RuO}_4$ , *Phys. Rev. Res.* **3**, 023067 (2021).

- [32] S. Y. Song, J. H. J. Martiny, A. Kreisel, B. M. Andersen, and J. Seo, Visualization of local magnetic moments emerging from impurities in Hund's metal states of FeSe, *Phys. Rev. Lett.* **124**, 117001 (2020).
- [33] J. Villain, Insulating spin glasses, *Z. Phys. B* **33**, 31 (1979).
- [34] J. Villain, R. Bidaux, J.-P. Carton, and R. Conte, Order as an effect of disorder, *J. Phys. France* **41**, 1263 (1980).
- [35] A. B. Harris, C. Kallin, and A. J. Berlinsky, Possible Néel orderings of the kagomé antiferromagnet, *Phys. Rev. B* **45**, 2899 (1992).
- [36] J. T. Chalker, P. C. W. Holdsworth, and E. F. Shender, Hidden order in a frustrated system: Properties of the Heisenberg kagomé antiferromagnet, *Phys. Rev. Lett.* **68**, 855 (1992).
- [37] A. Chubukov, Order from disorder in a kagomé antiferromagnet, *Phys. Rev. Lett.* **69**, 832 (1992).
- [38] E. F. Shender and P. C. W. Holdsworth, in *Fluctuations and Order: The New Synthesis*, edited by M. Millonas (Springer, New York, 1996), pp. 259–279.
- [39] D. Bergman, J. Alicea, E. Gull, S. Trebst, and L. Balents, Order-by-disorder and spiral spin-liquid in frustrated diamond-lattice antiferromagnets, *Nat. Phys.* **3**, 487 (2007).
- [40] A. G. Green, G. Conduit, and F. Krüger, Quantum order-by-disorder in strongly correlated metals, *Annu. Rev. Condens. Matter Phys.* **9**, 59 (2018).
- [41] Y. Tan, T. Zhang, T. Zou, A. M. dos Santos, J. Hu, D.-X. Yao, Z. Q. Mao, X. Ke, and W. Ku, Stronger quantum fluctuation with larger spins: Emergent magnetism in the pressurized high-temperature superconductor FeSe, *Phys. Rev. Res.* **4**, 033115 (2022).
- [42] Y.-T. Tam, D.-X. Yao, and W. Ku, Itinerancy-enhanced quantum fluctuation of magnetic moments in iron-based superconductors, *Phys. Rev. Lett.* **115**, 117001 (2015).
- [43] M. A. Ruderman and C. Kittel, Indirect exchange coupling of nuclear magnetic moments by conduction electrons, *Phys. Rev.* **96**, 99 (1954).
- [44] G. I. Japaridze and A. P. Kampf, Weak-coupling phase diagram of the extended Hubbard model with correlated-hopping interaction, *Phys. Rev. B* **59**, 12822 (1999).
- [45] P. W. Anderson, Absence of diffusion in certain random lattices, *Phys. Rev.* **109**, 1492 (1958).
- [46] A. Jagannathan, E. Abrahams, and M. J. Stephen, Magnetic exchange in disordered metals, *Phys. Rev. B* **37**, 436 (1988).
- [47] L. Bulaevskii and S. Panyukov, RKKY interaction in metals with impurities, *JETP Lett.* **43**, 240 (1986).
- [48] J. A. Sobota, D. Tanasković, and V. Dobrosavljević, RKKY interactions in the regime of strong localization, *Phys. Rev. B* **76**, 245106 (2007).
- [49] B. Keimer, S. A. Kivelson, M. R. Norman, S. Uchida, and J. Zaanen, From quantum matter to high-temperature superconductivity in copper oxides, *Nature (London)* **518**, 179 (2015).
- [50] H. Hosono, A. Yamamoto, H. Hiramatsu, and Y. Ma, Recent advances in iron-based superconductors toward applications, *Mater. Today* **21**, 278 (2018).
- [51] F. C. Zhang and T. M. Rice, Effective hamiltonian for the superconducting Cu oxides, *Phys. Rev. B* **37**, 3759 (1988).
- [52] J. Zaanen and A. M. Oleś, Canonical perturbation theory and the two-band model for high- $T_c$  superconductors, *Phys. Rev. B* **37**, 9423 (1988).
- [53] M. Lavagna and C. Pepin, The Kondo lattice model, *Acta Phys. Pol. B* **29**, 3753 (1998).
- [54] M. Kirčan and M. Vojta, Magnetic order in lightly doped cuprates: Coherent versus incoherent hole quasiparticles and nonmagnetic impurities, *Phys. Rev. B* **73**, 014516 (2006).
- [55] W.-G. Yin, C.-C. Lee, and W. Ku, Unified picture for magnetic correlations in iron-based superconductors, *Phys. Rev. Lett.* **105**, 107004 (2010).
- [56] W. Lv, F. Krüger, and P. Phillips, Orbital ordering and unfrustrated  $(\pi, 0)$  magnetism from degenerate double exchange in the iron pnictides, *Phys. Rev. B* **82**, 045125 (2010).
- [57] S.-P. Kou, T. Li, and Z.-Y. Weng, Coexistence of itinerant electrons and local moments in iron-based superconductors, *Europhys. Lett.* **88**, 17010 (2009).
- [58] S. Liang, G. Alvarez, C. Şen, A. Moreo, and E. Dagotto, Anisotropy of electrical transport in pnictide superconductors studied using Monte Carlo simulations of the spin-fermion model, *Phys. Rev. Lett.* **109**, 047001 (2012).
- [59] P. W. Anderson, An approximate quantum theory of the antiferromagnetic ground state, *Phys. Rev.* **86**, 694 (1952).
- [60] T. Holstein and H. Primakoff, Field dependence of the intrinsic domain magnetization of a ferromagnet, *Phys. Rev.* **58**, 1098 (1940).
- [61] It is easy to verify that any other ordered states would suffer even more fluctuation, in both short and long range [41,42] as long as the reconstructed Fermi surface remains.
- [62] T. Berlijn, H.-P. Cheng, P. J. Hirschfeld, and W. Ku, Doping effects of Se vacancies in monolayer FeSe, *Phys. Rev. B* **89**, 020501(R) (2014).
- [63] L. Wang, T. Berlijn, Y. Wang, C.-H. Lin, P. J. Hirschfeld, and W. Ku, Effects of disordered Ru substitution in BaFe<sub>2</sub>As<sub>2</sub>: Possible realization of superdiffusion in real materials, *Phys. Rev. Lett.* **110**, 037001 (2013).
- [64] T. Berlijn, P. J. Hirschfeld, and W. Ku, Effective doping and suppression of fermi surface reconstruction via Fe vacancy disorder in K<sub>x</sub>Fe<sub>2-y</sub>Se<sub>2</sub>, *Phys. Rev. Lett.* **109**, 147003 (2012).
- [65] T. Berlijn, D. Volja, and W. Ku, Can disorder alone destroy the  $e'_g$  hole pockets of Na<sub>x</sub>CoO<sub>2</sub>? A Wannier function based first-principles method for disordered systems, *Phys. Rev. Lett.* **106**, 077005 (2011).
- [66] C. Tsallis, Diagonalization methods for the general bilinear hamiltonian of an assembly of bosons, *J. Math. Phys.* **19**, 277 (1978).
- [67] W. Ku, T. Berlijn, and C.-C. Lee, Unfolding first-principles band structures, *Phys. Rev. Lett.* **104**, 216401 (2010).